ACS APPLIED MATERIALS & INTERFACES

Research Article

www.acsami.org

High-Resolution Organic Light-Emitting Diodes Patterned via Contact Printing

Jinhai Li, Lisong Xu, Ching W. Tang, and Alexander A. Shestopalov*

Department of Chemical Engineering, University of Rochester, Rochester, New York 14627, United States

Supporting Information

ABSTRACT: In this study, we report a contact printing technique that uses polyurethane-acrylate (PUA) polymers as the printing stamps to pattern electroluminescent layers of organic light emitting diodes (OLEDs). We demonstrate that electroluminescent thin films can be printed with high uniformity and resolution. We also show that the performance of the printed devices can be improved via postprinting thermal annealing, and that the external quantum efficiency of the printed devices is comparable with the efficiency of the vacuum-deposited OLEDs. Our results suggest that the PUA-based contact printing can be used as an alternative to the traditional shadow mask deposition, permitting manufacturing of OLED displays with the resolution up to the diffraction limit of visible-light emission.

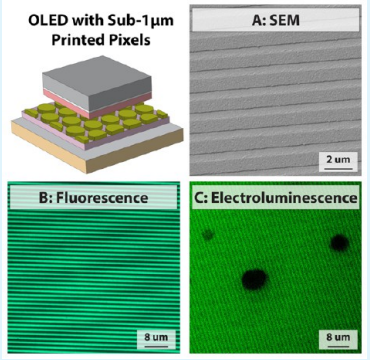

KEYWORDS: *contact printing, polyurethane acrylate, thin-film patterning, organic light emitting diodes, high-resolution printing*

INTRODUCTION

Contact printing is a patterning method that relies on the interfacial material transfer from an elastic stamp to a hard or soft substrate. Because of its simplicity, contact printing is often considered as the method of choice for additive micro- and nanoscale manufacturing of multilayered thin-film devices.[1−6] Several studies have demonstrated successful thin film patterning of electronic components using simple interfacial material transfer with elastic polydimethylsiloxane (PDMS) stamps. Despite its many advantages, a few limitations of the PDMS-based printing remain, specifically (i) relatively large feature sizes (tens of micrometers) due to the distortion and deformation of the low modulus PDMS stamps,[7,8] (ii) limited control over the interfacial adhesion due to the constant hydrophobic nature of PDMS,[9−11] and (iii) reduced efficiency of the fabricated devices due to the low quality of the printed interfacial contacts.[4,12] In addition, thin film delamination/deposition mechanics in the PDMS-based printing is typically regulated by the rate-dependent effects of viscoelastic PDMS stamps.[13−17] Such rate-dependent modulation of thin film adhesion requires careful optimization and control of the stamping velocity for each new printing material, and so far it has been primarily used for printing large 50−100 μm features.

Traditional OLED microdisplays use large-area white pixels with patterned color filters to produce RGB subpixels. The filters reduce light transmission by ∼80%, lowering efficiency. Direct deposition of RGB emitters via shadow mask deposition through the standard fine metal mask (FMM) directly deposits and aligns individual color pixels, avoiding the transmission loss. However, FMM-based patterning has a limited resolution (>10 μm) due to the material diffusion in the gap between the mask and the substrate.[18,19] Because contact printing directly transfers materials between interfaces, it avoids the diffusive limitation of the shadow mask deposition. Beyond resolution, contact printing offers two other major advantages: (1) FMMs are very difficult to scale up to large and curvilinear substrates and they are more expensive to replace compared to simple polymeric molds, and (2) shadow-masks block a large fraction of evaporated material and require frequent cleaning, leading to significant waste of organic semiconducting materials and high production cost. Previously, the PDMS-based printing was used to structure OLED components. For example, spin-coated organic electroluminescent layers were directly transferred from the PDMS stamp to create functional multilayered OLED devices.[20,21] These studies demonstrated that different emitters can be used to create continuous OLEDs[20] and patterned OLED chips with ∼150 μm electroluminescent pixels.[21] However, the efficiency of the printed devices was not compared to the standard vacuum-deposited OLEDs, and it was noted, that the poor integrity of the printed films can lead to a low device performance.[20] In another study, a flat thin PDMS layer supported on the rigid backplane was used to indirectly pattern 12 μm × 40 μm OLED pixels. It was demonstrated, that the JV characteristics of the printed and spin-coated devices with continuous emitting layers are comparable, but no comparison between the patterned devices and devices fabricated in vacuum was provided.[22] Other works in this area included patterning of >10 μm OLED pixels via

Received: May 3, 2016
Accepted: June 15, 2016
Published: June 15, 2016

DOI: 10.1021/acsami.6b05286
ACS Appl. Mater. Interfaces 2016, 8, 16809−16815

kinetically modulated quick release PDMS lift-off printing,[23] and physical lamination of top OLED metal electrodes supported on the PDMS layer against electroluminescent pixels.[24] To the best of our knowledge, there exist no examples of using contact printing to manufacture efficient OLEDs with pixels smaller than 10 μm.

Recently, we demonstrated that several limitations of the PDMS-based printing can be obviated by replacing PDMS with polyurethane-acrylate (PUA) elastomers. Specifically, we showed that by controlling surface polarity and stiffness of the PUA stamps, micrometer and submicrometer structures of organic monolayers and thin films can be replicated with high resolution and uniformity.[25] However, our study revealed that the resulting OLEDs with printed pixels have low external quantum efficiencies (EQEs) and numerous nonemitting black areas. In that study we also investigated the relationship between the PUA composition, its physical properties and printing efficiency. Dynamic mechanical analysis demonstrated that the storage modulus of PUA polymers decreases with temperature and reaches minimum rubbery plateau at around 40−50 °C. We also examined the dependence of the adhesion of the PUA stamps on the applied pressure and temperature. We showed that the pull-off force of the patterned PUA stamps decreases as the temperature increases from 25 to 40 °C, and that it remains largely constant in the 40−75 °C range. We contributed the initial decrease of the pull-off force to the transition of the polymer from a semiglassy to a rubbery state at 35−45 °C. We also demonstrated that there is a minimal applied force that must be attained to achieve the highest possible adhesion, and that the further increase in the applied pressure does not change the force of adhesion. Our collective measurements suggest that the optimal printing temperature for the PUA polymers should be higher than 50 °C when it completely transition into the low adhesion, rubbery regime.

Here, we demonstrate that by optimizing printing conditions and via postprinting annealing the interlayer uniformity of the printed OLED layers can be improved leading to devices with significantly reduced number of nonemitting defects. We also show that the devices with the printed electroluminescent layers are comparable to the vapor-deposited OLEDs in efficiency and JV parameters. Finally, we demonstrate that the PUA-based contact printing can be used to pattern submicrometer pixels of the functional OLED devices providing a plausible pathway for manufacturing superhigh resolution OLEDs.

RESULTS AND DISCUSSION

OLED Printing. In this study we used standard materials and architecture for comparison of the printed and vacuum-deposited OLEDs. All reported OLEDs had the following architecture (Figure 1): cathode: indium tin oxide (ITO) on glass; hole injection layer (HIL): 1 nm molybdenum oxide (MoOx); hole transport layer (HTL): 30 nm 1,4,7-triazacyclononane-*N*,*N*′,*N*″-triacetate (TCTA); emitter layer (EML): 20 nm tris[2-phenylpyridinato-C2,*N*]iridium(III) (Ir(ppy)$_3$ hosted in TCTA; electron transport layer (ETL): 30 nm bathophenanthroline (BPhen); electron injection layer (EIL): 1 nm lithium fluoride (LiF); cathode: 100 nm aluminum. We first determined how the concentration of Ir(ppy)$_3$ dopant in the host TCTA layer affects the external quantum efficiency (EQE) of the vacuum deposited devices. The EQE increased with the dopant concentration from 1 to 9% and then decreased at concentrations higher than 11% (Figure S1). Accordingly, we used 10% of Ir(ppy)$_3$ in TCTA as the EML in all subsequent experiments.

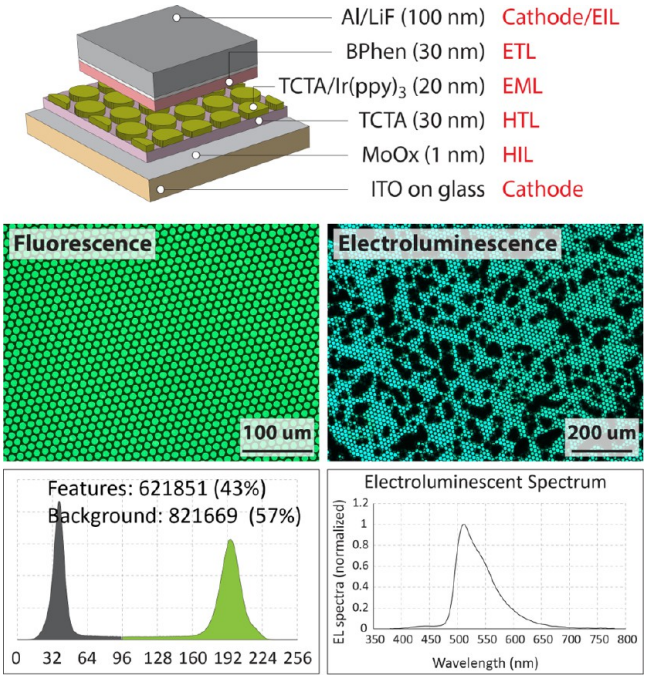

Figure 1. Top illustration: OLED structure and components; middle micrographs: fluorescent and electroluminescent micrographs of the printed EML dots and the corresponding OLED device; bottom plots: fluorescent histogram with feature-to-background surface area ratio and electroluminescent spectrum of the OLED device.

Printed OLEDs were prepared by using PUA polymer (Figure S2) as a contact printing stamp to replicate a pattern of the EML layer. The pattern is consisted of 8 μm hexagonal dots printed on the vapor-deposited TCTA HTL film. The PUA stamps were prepared by replica molding from the silicon/silicon oxide master following previously published methods.[26,27] Subsequently, a thin layer (20 nm) of TCTA/Ir(ppy)$_3$ was vapor-deposited on the stamp surface. The initial printing was conducted at 80 °C for 10 min in air under a constant load of 110 kPa. These conditions were selected from our previous studies.[25] Printed substrates were analyzed via fluorescent microscopy or used to prepare OLED devices. Figure 1 shows that the fluorescent pattern of the printed TCTA/Ir(ppy)$_3$ layer was replicated accurately on the entire substrate area (imaged in at least three different areas). The fluorescent histogram shows that the background-to-feature ratio (57:43%) of the printed layers correlates well with the corresponding ratio on the original silicon master (56:44%, Figure S3). Previously, we demonstrated using X-ray photoelectron spectroscopy (XPS) that the selected printing conditions yield a complete transfer of the organic thin films from the stamp to the substrate.[25] To evaluate the properties of the printed contacts we examined the electroluminescent pattern of the completed OLEDs, which were prepared by vapor-depositing layers of BPhen, LiF and Al on top of the printed Ir(PPy)$_3$/TCTA **EML** layer. The electroluminescent spectrum confirmed light emission from Ir(ppy)$_3$ of the **EML**. The electroluminescent micrograph contained numerous continuous, circular or oval shaped dark spots (Figures 1 and Figure S3). These nonemissive defects, which have been attributed to moisture-induced cathode degradation or corrosion, are more numerous in the printed OLEDs than in vacuum-deposited OLEDs. This excessive

DOI: 10.1021/acsami.6b05286
ACS Appl. Mater. Interfaces 2016, 8, 16809−16815

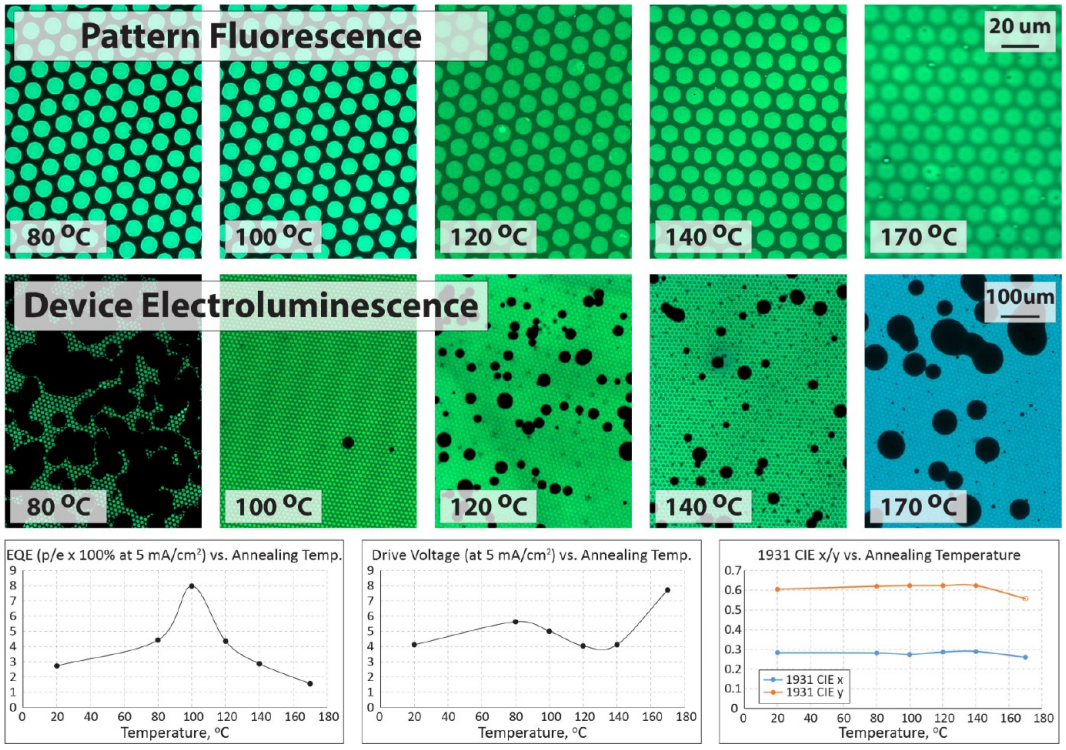

Figure 2. Thermal annealing of the printed EML patterns. Top micrographs: fluorescent patterns of the printed EML pixels; middle micrographs: electroluminescent patterns of the corresponding devices; bottom: device parameters (we note that some of the fluorescent micrographs contain small dust particles, which are inevitable in a typical laboratory environment).

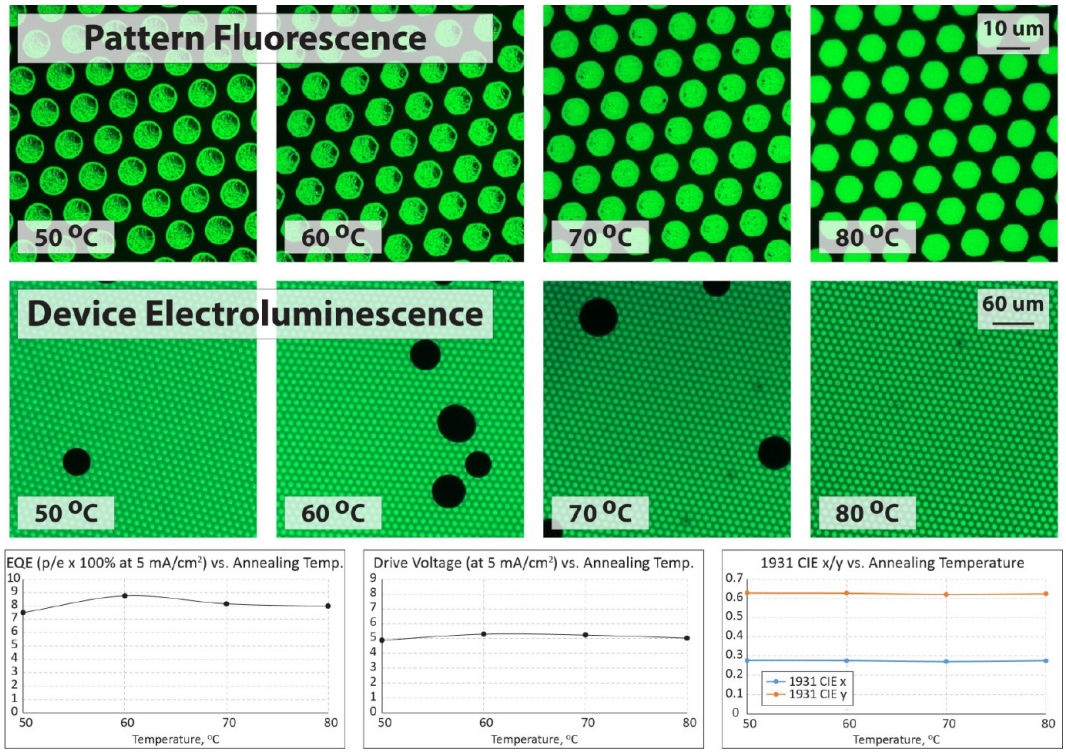

Figure 3. EML pixels printed at different temperatures. Top micrographs: fluorescent patterns of the printed EML pixels; middle micrographs: electroluminescent patterns of the corresponding devices; bottom: device parameters.

growth of dark spots can be attributed to the current process of EML printing in air without taking steps to preclude moisture. The differential in adhesion strength between the various layers may also result in separation of the layers during the stamp removal, consequently producing topological defects that promote dark spot growth.

Optimization of the Printing Conditions. To reduce nonemissive defects in the printed OLEDs, we experimented

DOI: 10.1021/acsami.6b05286
ACS Appl. Mater. Interfaces 2016, 8, 16809−16815

with the postprinting annealing conditions. In these experiments, a set of identical substrates (with the printed **EML** on the **HTL** layer) were annealed for 10 min in nitrogen atmosphere at different temperatures (80, 100, 120, 140, and 170 °C) and imaged with fluorescent microscopy using constant exposure settings. Thermal annealing at an appropriate temperature can improve the adhesion between the layers through van der Waals interactions by softening the OLED components, or it can remove moisture that remains on the substrates after the printing and air exposure. However, annealing above 150 °C (the glass transition temperature of TCTA[28]) is expected to cause pattern deformation and possibly photoinduced degradation of $Ir(ppy)_3$, which can be accelerated by higher temperatures.[29] Following the annealing, 30 nm of BPhen, 1 nm of LiF, and 100 nm of Al were deposited in vacuum to complete the devices.

Fluorescence micrographs of the annealed samples show that annealing at 80 and 100 °C does not lead to noticeable changes in the printed patterns (Figure 2). At these temperatures, they were identical to the patterns without the annealing (Figure 1). However, annealing at 120 and 140 °C resulted in a noticeable loss in fluorescent contrast. Annealing at 170 °C produced low contrast fluorescent patterns with deformed (widened) features, indicating possible material degradation and diffusive spreading.

The electroluminescent images demonstrate that annealing at 100 °C produce OLEDs with a significantly reduced number of the dark spots whereas annealing at 80 °C (same as the printing temperature) did not cause any significant changes. However, annealing at higher temperatures, 120 °C, 140 and 170 °C, produced patterns with a lower electroluminescent contrast. Annealing at 170 °C also caused noticeable electroluminescent color shift. These findings were further supported by the measured OLED parameters (Figure 2). The external quantum efficiency (EQE) of the fabricated devices was the highest for the device annealed at 100 °C. The same device also showed more accurate and uniform fluorescent and electroluminescent patterns. The device annealed at 170 °C demonstrated the lowest EQE, the highest drive voltage, and showed substantial changes in 1931 CIE x/y color parameters (color shift from green to blue), which suggest possible material degradation or a shift in the recombination zone due to the vertical diffusion between the **HTL** and **EML** layers. These experiments suggest that postprinting annealing at 100 °C leads to reduction of dark spot defects and an overall improvement in OLED device performance.

Subsequently, we examined how the printing temperature affects the pattern resolution and OLED device parameters. Previously, we have demonstrated that the PUA stamps can accurately replicate organic thin film patterns at or slightly above a printing temperature of 80 °C. Here, we examined printing temperatures at 50, 60, 70, and 80 °C, followed by annealing at 100 °C in nitrogen as in previously described conditions (Figure 3). The fluorescent images of the printed patterns were taken before the annealing step.

The electroluminescent images of the completed OLED devices and the measured device parameters contain no significant differences between the devices, suggesting that printing temperatures up to 80 °C do not cause material degradation. However, the fluorescent images show that printing at 50 and 60 °C produces patterns with nonuniform distribution of the EML material within the individual features. These features contain black areas whose arrangement appears to have certain orientation. The fact that the completed OLED devices showed no noticeable differences (including uniform electroluminescence) would suggest that the Young's modulus of the PUA stamp at low printing temperatures remains too high to achieve a uniform contact pressure distribution. Fluorescent micrographs show that printing at 80 °C achieves the best intensity contract between the fluorescent features and nonfluorescent background (Figure 3). These experiments and our prior results[25] suggest that at a printing temperature of 80 °C, the PUA stamp achieves optimal elasticity for uniform replication of features with microscopic dimensions. It should be noted that the optimal modulus may be different for features with different dimensions.

The printed EML patterns were also examined with SEM and AFM to determine their surface roughness and resolution. SEM images (Figure 4) demonstrate that the printed patterns

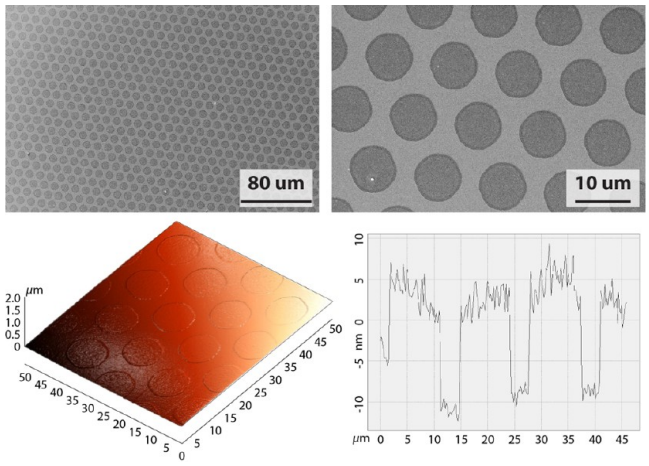

Figure 4. Top: SEM images of the printed EML pixels; bottom: AFM image and height profile of the printed EML pixels.

are uniform and free of surface cracks and stamping artifacts. These results are in the agreement with our previous work that demonstrated that inactive PUA stamps do not contaminate interfaces with debris or stamp marks, and that they afford clean and accurate pattern transfer with sub-100 nm resolution when used in molecular or catalytic printing.[26,27,30−32] SEM analysis also revealed that the chemical composition of the EML (TCTA/Ir(PPy)) patterns is different from the HTL (TCTA) background. AFM analysis showed that the printed features have the same roughness as the background area. The AFM height profile shows that the edge resolution of the printed features is below 1 μm, suggesting the possibility of accurately replicating submicrometer objects. We note, however, that SEM and AFM imaging cannot probe the quality of the printed contacts and can only be used to assess the surface properties of the printed features.

Comparison of Printed and Vacuum-Deposited OLEDs. We compared the performance of OLED devices fabricated via contact printing and vacuum deposition. Because our vacuum-deposited devices contain continuous emitting layers, they cannot be directly compared to the patterned OLEDs where the EML is noncontinuous. To estimate the efficiency of a hypothetical vacuum-deposited device (Figure 5, PV) that has the same 43:57 ratio of the emitting and background areas as the printed OLED (PP), we measured parameters of two nonpatterned, vacuum-deposited OLEDs with (EV) and without (BV) the emitting layer. The

DOI: 10.1021/acsami.6b05286
ACS Appl. Mater. Interfaces 2016, 8, 16809−16815

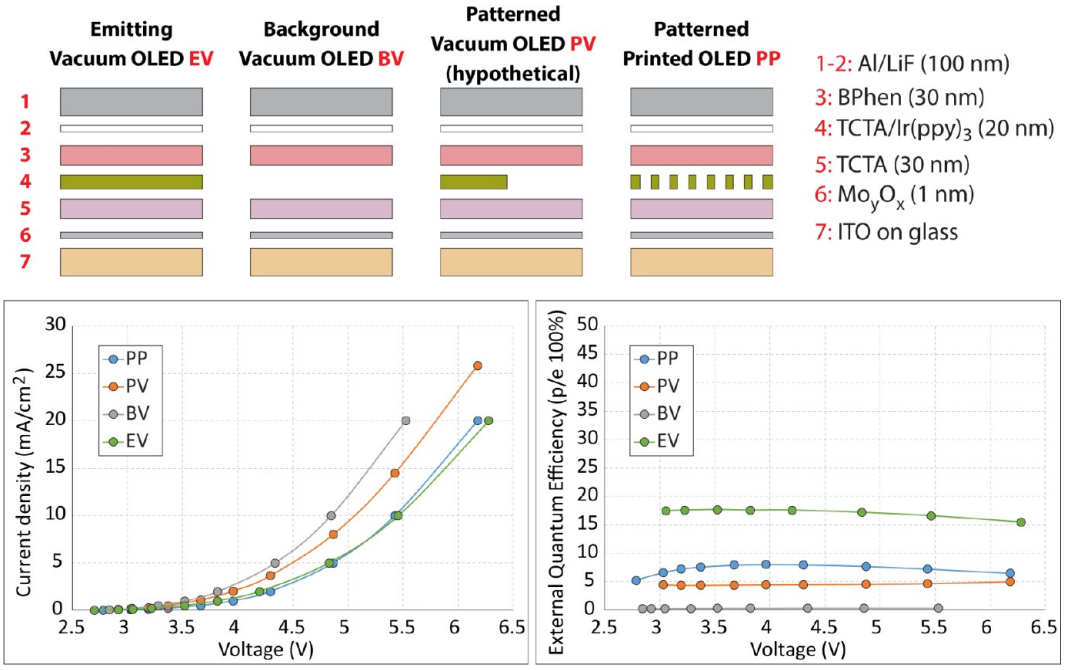

Figure 5. Current density and external quantum efficiency of the printed (PP), and vacuum-deposited OLED devices (EV, BV, and PV).

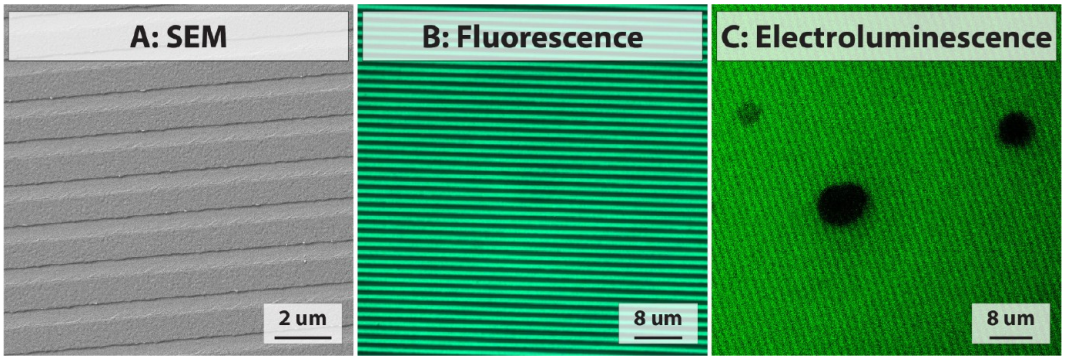

Figure 6. (A) SEM image of the printed and annealed EML lines (5 nm Au metallization); (B) fluorescent image of the printed and annealed EML lines; (C) electroluminescent image of the corresponding OLED.

compositions and structures of these reference OLEDs are identical to the emitting and background areas in the printed device (PP), with the exception that all the layers were deposited via vacuum deposition. First, the current–voltage dependencies of the reference devices (EV and BV) were plotted and fitted into the polynomial equations to calculate current densities of the hypothetical PV OLED at the voltages of the printed device (PP). JV plots of the PV and PP devices show that at the same voltage the vacuum-deposited device has higher current density (lower resistance) than the printed OLED. We then calculated spectral radiances of the hypothetical PV device at the voltages of the PP device, using linear fits of the radiance vs current density plots of the reference EV and BV OLEDs. Finally, the calculated current densities and spectral radiances of the PV OLED were used to calculate its EQE (see Figures S4–S6 for more details).

Figure 5 shows that the EQE values of the printed PP device are similar and slightly higher than EQE's of the hypothetical, vacuum-deposited PV OLED. This comparison suggests that contact printing and thermal annealing can produce interfacial contacts of similar quality with the traditional vacuum deposition. One potential explanation for slightly higher EQE values of the printed PP device is the difference in the light outcoupling efficiency of planar and microstructured layers.

Printed OLEDs with Submicrometer Features. Because of its potential advantages in terms of the manufacturing cost, scalability, and ability to pattern on curved and flexible substrates, contact printing is a desirable alternative to vacuum deposition in fabricating OLED devices. A major concern for contact printing has been the performance of the printed devices, which are generally inferior to equivalent vacuum-deposited devices. Our preliminary results show that by selecting appropriate stamping materials and by optimizing patterning conditions such as printing and annealing temperatures, printed OLED devices can have similar efficiencies and defect amounts as the vacuum deposited OLED devices. Another potential advantage of the contact printing is the ability to replicate submicrometer patterns.

To show advantages of our contact printing in submicrometer thin film patterning, we used PUA stamps to patterns 900 nm lines of light-emitting layers separated by 550 nm. The arrays of microgroves on a blank polycarbonate CD disc was used as the master to prepare PUA stamps containing patterns of parallel lines. We deposited 20 nm of TCTA with 10%

DOI: 10.1021/acsami.6b05286
ACS Appl. Mater. Interfaces 2016, 8, 16809–16815

$Ir(ppy)_3$ by vacuum deposition on the patterned PUA surface and used this stamp in contact printing with the ITO/MoOx/TCTA substrate (same device architecture as in the previous experiments). The inked stamp was brought into conformal contact with the substrate under vacuum at 40 °C for 10 min. Printing at higher temperatures resulted in degraded resolution, possibly due to the deformations of the small features caused by the softening of the PUA elastomer. This observation is in the agreement with the literature data,[7,8,26,27] which shows that smaller features typically require stamp elastomers with higher Young's modulus to be accurately reproduced on rigid substrates. Because PUA storage modulus can be changed from 9×10^7 to 2×10^7 Pa in the 20−70 °C temperature range,[25] our stamp material provides the ability to replicate both microscopic and nanoscopic patterns at the printing temperatures that do not cause degradation of typical organic electronic materials.

Fluorescent and SEM images of the patterns printed at 40 °C and annealed at 100 °C show that the printed features have dimensions and edge registrations comparable with the original CD pattern (Figures 6A, B and Figure S4). Subsequently, printed and annealed submicrometer patterns of 20 nm of TCTA with 10% $Ir(ppy)_3$ were used to fabricate OLED devices (same device architecture as in the previous experiments). Figure 6C shows the electroluminescent pattern of the prepared device. The total thickness of the fabricated device and the small working distance of the 50× and 100× objectives prevented us from obtaining high-resolution electroluminescent images. Nonetheless, Figure 6C clearly confirms the presence of patterned lines and shows that the fabricated device has a small number of dark spot defects. These initial results show that high-resolution OLED displays (1.4 μm pixel+pitch dimension) are potentially attainable via the PUA-based contact printing. However, many other problems such as high-resolution pattern alignment with soft polymeric stamps, top inorganic electrode interconnection without shadow mask processing, and submicrometer photolithographic patterning of curved and large-area TFT matrices have to be independently solved before such devices will become a reality.

CONCLUSIONS

Our study demonstrates that the PUA polymers can be used as contact printing stamps to pattern semiconducting organic thin films. We have demonstrated that the electroluminescent layers of organic light emitting diodes can be patterned using PUA-based printing with good uniformity (without printing defects over 3×3 mm^2 area) and resolution (900 nm lines separated by 550 nm). The reported resolution exceeds the current limit of the traditional shadow mask deposition, and, in theory, permits manufacturing of OLEDs with dpi values approaching a theoretical diffraction limit for the resolved emission from the two adjacent pixels. Our study also shows that the efficiency of the OLEDs containing printed components can be improved via thermal annealing and made similar to the EQE's of the vacuum-deposited devices. We showed that the thermal annealing does not cause the degradation of the organic thin films, and that it does not lead to the geometrical distortion of the printed features. Together, our results serve as a firm foundation for exploring PUA-based printing in the patterning of multicomponent thin film stacks and in manufacturing of full-color OLED displays.

ASSOCIATED CONTENT

Supporting Information

The Supporting Information is available free of charge on the ACS Publications website at DOI: 10.1021/acsami.6b05286.

Experimental details, characterization methods, and detailed comparison of the printed and vacuum-deposited OLEDs (PDF)

AUTHOR INFORMATION

Corresponding Author

*E-mail: alexander.shestopalov@rochester.edu.

Notes

The authors declare no competing financial interest.

ACKNOWLEDGMENTS

Financial support from the NSF (ECCS 1530540 and DMR 1228889) is gratefully acknowledged

REFERENCES

(1) Kim, D.-H.; Lu, N.; Ma, R.; Kim, Y.-S.; Kim, R.-H.; Wang, S.; Wu, J.; Won, S. M.; Tao, H.; Islam, A.; Yu, K. J.; Kim, T.-i.; Chowdhury, R.; Ying, M.; Xu, L.; Li, M.; Chung, H.-J.; Keum, H.; McCormick, M.; Liu, P.; Zhang, Y.-W.; Omenetto, F. G.; Huang, Y.; Coleman, T.; Rogers, J. A. Epidermal Electronics. *Science (Washington, DC, U. S.)* **2011**, *333* (6044), 838−843.

(2) Yeo, W.-H.; Kim, Y.-S.; Lee, J.; Ameen, A.; Shi, L.; Li, M.; Wang, S.; Ma, R.; Jin, S. H.; Kang, Z.; Huang, Y.; Rogers, J. A. Multifunctional Epidermal Electronics Printed Directly Onto the Skin. *Adv. Mater. (Weinheim, Ger.)* **2013**, *25* (20), 2773−2778.

(3) Takakuwa, A. Development of High Precision Patterning Technology by Using Micro-Contact Printing (μCP) Method, and Application to Organic TFT. *Mol. Electron. Bioelectron.* **2009**, *20* (2), 111−114.

(4) Carlson, A.; Bowen, A. M.; Huang, Y. G.; Nuzzo, R. G.; Rogers, J. A. Transfer Printing Techniques for Materials Assembly and Micro/Nanodevice Fabrication. *Adv. Mater. (Weinheim, Ger.)* **2012**, *24* (39), 5284−5318.

(5) Kim, D.-H.; Ghaffari, R.; Lu, N.; Rogers, J. A. Flexible and Stretchable Electronics for Biointegrated Devices. *Annu. Rev. Biomed. Eng.* **2012**, *14*, 113−128.

(6) Rogers, J. A.; Someya, T.; Huang, Y. Materials and Mechanics for Stretchable Electronics. *Science (Washington, DC, U. S.)* **2010**, *327* (5973), 1603−1607.

(7) Hui, C. Y.; Jagota, A.; Lin, Y. Y.; Kramer, E. J. Constraints on Microcontact Printing Imposed by Stamp Deformation. *Langmuir* **2002**, *18* (4), 1394−1407.

(8) Hwang, J. K.; Cho, S.; Dang, J. M.; Kwak, E. B.; Song, K.; Moon, J.; Sung, M. M. Direct Nanoprinting by Liquid-Bridge-Mediated Nanotransfer Moulding. *Nat. Nanotechnol.* **2010**, *5* (10), 742−748.

(9) Li, X. M.; Peter, M.; Huskens, J.; Reinhoudt, D. N. Catalytic microcontact printing without ink. *Nano Lett.* **2003**, *3* (10), 1449−1453.

(10) Owen, M. J.; Smith, P. J. Plasma Treatment of Polydimethylsiloxane. *J. Adhes. Sci. Technol.* **1994**, *8* (10), 1063−1075.

(11) Olander, B.; Wirsen, A.; Albertsson, A. C. Oxygen Microwave Plasma Treatment of Silicone Elastomer: Kinetic Behavior and Surface Composition. *J. Appl. Polym. Sci.* **2004**, *91* (6), 4098−4104.

(12) Khan, S.; Lorenzelli, L.; Dahiya, R. S. Technologies for Printing Sensors and Electronics Over Large Flexible Substrates: A Review. *IEEE Sens. J.* **2015**, *15* (6), 3164−3185.

(13) Meitl, M. A.; Zhu, Z.-T.; Kumar, V.; Lee, K. J.; Feng, X.; Huang, Y. Y.; Adesida, I.; Nuzzo, R. G.; Rogers, J. A. Transfer Printing by Kinetic Control of Adhesion to an Elastomeric Stamp. *Nat. Mater.* **2006**, *5* (1), 33−38.

(14) Baca, A. J.; Ahn, J.-H.; Sun, Y.; Meitl, M. A.; Menard, E.; Kim, H.-S.; Choi, W. M.; Kim, D.-H.; Huang, Y.; Rogers, J. A.

DOI: 10.1021/acsami.6b05286
ACS Appl. Mater. Interfaces 2016, 8, 16809−16815

Semiconductor Wires and Ribbons for High- Performance Flexible Electronics. *Angew. Chem., Int. Ed.* **2008**, *47* (30), 5524−5542.
(15) Sun, Y.; Kim, H.-S.; Menard, E.; Kim, S.; Adesida, I.; Rogers, J. A. Printed Arrays of Aligned GaAs Wires for Flexible Transistors, Diodes, and Circuits on Plastic Substrates. *Small* **2006**, *2* (11), 1330−1334.
(16) Sun, Y.; Rogers, J. A. Inorganic Semiconductors for Flexible Electronics. *Adv. Mater. (Weinheim, Ger.)* **2007**, *19* (15), 1897−1916.
(17) Kim, T.-H.; Choi, W. M.; Kim, D.-H.; Meitl, M. A.; Menard, E.; Jiang, H.; Carlisle, J. A.; Rogers, J. A. Printable, Flexible, and Stretchable Forms of Ultrananocrystalline Diamond with Applications in Thermal Management. *Adv. Mater. (Weinheim, Ger.)* **2008**, *20* (11), 2171−2176.
(18) Kummamuru, R. K.; Hu, L.; Cook, L.; Efremov, M. Y.; Olson, E. A.; Allen, L. H. A Close Proximity Self-Aligned Shadow Mask for Sputter Deposition onto a Membrane or Cavity. *J. Micromech. Microeng.* **2008**, *18* (9), 095027.
(19) Ling, M. M.; Bao, Z. Thin Film Deposition, Patterning, and Printing in Organic Thin Film Transistors. *Chem. Mater.* **2004**, *16* (23), 4824−4840.
(20) Chen, S.-Z.; Peng, S.-H.; Ting, T.-Y.; Wu, P.-S.; Lin, C.-H.; Chang, C.-Y.; Shyue, J.-J.; Jou, J.-H. Organic Light-Emitting Diodes with Direct Contact-Printed Red, Green, Blue, and White Light-Emitting Layers. *Appl. Phys. Lett.* **2012**, *101* (15), 153304.
(21) Park, T. H.; Park, Y. W.; Choi, J. H.; Choi, H. J.; Jeong, J.-W.; Song, E. H.; Choi, K. C.; Ju, B.-K. Contact Printing of the Emitting Layer for High Performance Multilayered Phosphorescent Organic Light-Emitting Diodes. *Org. Electron.* **2011**, *12* (6), 1063−1067.
(22) Jin, H.; Sturm, J. C. Super-High-Resolution Transfer Printing for Full-Color OLED Display Patterning. *J. Soc. Inf. Disp.* **2010**, *18* (2), 141−145.
(23) Yu, J.; Bulović, V. Micropatterning Metal Electrode of Organic Light Emitting Devices Using Rapid Polydimethylsiloxane Lift-off. *Appl. Phys. Lett.* **2007**, *91* (4), 043102.
(24) Lee, T.-W.; Zaumseil, J.; Bao, Z.; Hsu, J. W. P.; Rogers, J. A. Organic Light-Emitting Diodes Formed by Soft Contact Lamination. *Proc. Natl. Acad. Sci. U. S. A.* **2004**, *101* (2), 429−433.
(25) Li, J.; Xu, L.; Kim, S.; Shestopalov, A. Urethane-Acrylate Polymers in High-Resolution Contact Printing. *J. Mater. Chem. C* **2016**, *4*, 4155−4165.
(26) Shestopalov, A. A.; Clark, R. L.; Toone, E. J. Inkless Microcontact Printing on Self-Assembled Monolayers of Fmoc-Protected Aminothiols. *J. Am. Chem. Soc.* **2007**, *129* (45), 13818−13819.
(27) Shestopalov, A. A.; Clark, R. L.; Toone, E. J. Inkless Microcontact Printing on SAMs of Boc- and TBS-Protected Thiols. *Nano Lett.* **2010**, *10* (1), 43−46.
(28) Chopra, K. L.; Major, S.; Pandya, D. K. Transparent Conductors—A Status Review. *Thin Solid Films* **1983**, *102* (1), 1−46.
(29) Schmidbauer, S.; Hohenleutner, A.; König, B. Studies on the Photodegradation of Red, Green and Blue Phosphorescent OLED Emitters. *Beilstein J. Org. Chem.* **2013**, *9*, 2088−2096.
(30) Bowers, C. M.; Zhang, M.; Lyubarskaya, Y.; Toone, E. J.; Tang, C.; Shestopalov, A. A. Structural Modifications in Bilayered Molecular Systems Lead to Predictable Changes in Their Electronic Properties. *Adv. Mater. Interfaces* **2014**, *1* (2), 1300109.
(31) Shestopalov, A. A.; Clark, R. L.; Toone, E. J. Catalytic Microcontact Printing on Chemically Functionalized H-Terminated Silicon. *Langmuir* **2010**, *26* (3), 1449−1451.
(32) Shestopalov, A. A.; Morris, C. J.; Vogen, B. N.; Hoertz, A.; Clark, R. L.; Toone, E. J. Soft-Lithographic Approach to Functionalization and Nanopatterning Oxide-Free Silicon. *Langmuir* **2011**, *27* (10), 6478−6485.

DOI: 10.1021/acsami.6b05286
ACS Appl. Mater. Interfaces 2016, 8, 16809−16815